Energy balance and evaporation loss of an agricultural reservoir in a semiarid climate (South-Eastern Spain)

B. Gallego-Elvira[1], A. Baille[1*], B. Martín-Górriz[1] and V. Martínez-Álvarez[1]

[1)]Technical University of Cartagena. Agricultural Engineering Section. Paseo Alfonso XIII, 48. 30203 Cartagena (Spain).

**Correspondence to: Alain Baille. Technical University of Cartagena. Agricultural Engineering Section. Paseo Alfonso XIII, 48. 30203 Cartagena (Spain). E-mail: Alain.baille@upct.es*

Abstract

A typical agricultural water reservoir (AWR) of 2400 m^2 area and 5 m depth, located in a semiarid area (southern Spain), was surveyed on a daily basis for one year. The annual evaporation flux was 102.7 W m^{-2}, equivalent to an evaporated water depth of 1310 mm $year^{-1}$. The heat storage rate G exhibited a clear annual cycle with a peak gain in April (G ~ 45 W m^{-2}) and a loss peak in November (G ~ 40 W m^{-2}), leading to a marked annual hysteretic trend when evaporation (λE) was related to net radiation (R_n). λE was strongly correlated with the available energy, A, representing 91% of the annual AWR energy loss. The sensible heat flux, H, accounted for the remaining 9%, leading to an annual Bowen ratio in the order of 0.10. The equilibrium and advective evaporation terms of the Penman formula represented 76% and 24%, respectively, of the total evaporation, corresponding to a annual value of the Priestley-Taylor (P-T) coefficient (α) of 1.32. The P-T coefficient presented a clear seasonal pattern, with a minimum of 1.23 (July) and a maximum of 1.65 (December), indicating that, during periods of limited available energy, AWR evaporation increased above the potential evaporation as a result of the advection process. Overall, the results stressed that accurate prediction of monthly evaporation by means of the P-T formula requires accounting for both the annual cycle of storage and the advective component. Some alternative approaches to estimating R_n, G and α are proposed and discussed.

KEY WORDS: Heat storage, energy partitioning, Bowen ratio, Priestley-Taylor formula.

INTRODUCTION

Free water surface evaporation is a major component of the hydrological cycle and needs to be evaluated for many issues related with irrigation management and water resources planning. Small water storages for livestock, fishing, irrigation or recreational activities are estimated to cover about 77,000 km^2 worldwide (Downing *et al*., 2006). In dry regions, where water availability varies seasonally, agricultural water reservoirs for irrigation (AWR) are commonly used to guarantee water supplies throughout the irrigation season (Ali *et al*., 2008; Martinez *et al*., 2006; Daigo and Phaovattana, 1999). Typical AWRs are characterized by a large area-to-volume ratio that implies substantial loss through evaporation, often representing a significant fraction of the total water managed during the irrigation season, especially in areas with a high evaporative demand (Hudson, 1987; Martinez *et al*., 2007). Craig *et al.* (2005) estimated that in many areas of Australia up to 40% of the stored water in on-farm storages might be lost through evaporation. By means of a physically-based model coupled to a geographical information system, Martínez *et al*. (2008) simulated the regional evaporation loss of AWRs in the Segura Basin (south-eastern Spain). The annual losses were estimated to be 58 hm^3, which represents 8.3% of the total agricultural water resources. These figures underline the importance of accurately estimating free water evaporation (E) from AWRs for assessing storage efficiency and for evaluating the use of mitigation measures, such as shade-cloth covers, which have been shown to substantially increase storage efficiency, with reductions in water loss of more than 80% (Martinez *et al*., 2006).

However, in spite of the increasing interest in optimising storage efficiency in irrigation districts, detailed evaporation studies of small water bodies are scarce and often based on sparse or remotely collected data (Rosenberry *et al*., 2007). To our knowledge, there are very few studies that provide a detailed insight into the dynamics of the energy balance components and evaporation loss of on-farm water reservoirs. Obviously, there is a need to better understand and for modelling evaporation processes from storage reservoirs or small dams. In particular, knowledge of the thermal storage in the water body and advection from surroundings is required to improve the prediction of evaporation (Finch, 2001; Finch and Gash, 2002; Gianniou and Antonopoulos, 2007; Sacks *et al.*, 1994). These factors are especially relevant when applying physically-based evaporation models, such as the well-known Penman combination equation

(Penman, 1948) or its truncated version, the Priestley-Taylor formula (Priestley and Taylor, 1972). Both methods require estimating (i) the available energy at the water surface (i.e. net radiation plus heat storage rate) and (ii) the relative importance of the advective component. The latter is quantified through the product of a wind function and vapour pressure deficit in the combination method, and by an advection coefficient in the Priestley-Taylor (P-T) equation. Thus, a thorough quantification and analysis of the components of the energy balance of a typical AWR based on detailed experimentation will provide a sound basis for assessing the performance of evaporation prediction methods, and particularly of the P-T formula, which is widely-used by hydrologists, climatologists and agronomists (McAneney and Itier, 1993).

PURPOSE OF THE STUDY

(i) To provide a complete description and quantification of the evaporation loss and the components of the surface energy balance from a typical on-farm AWR used in south eastern Spain through a one year survey carried out on a daily basis, (ii) to study the monthly energy partitioning, focusing on the evolution of the storage term, the advective component, the Bowen ratio and the available energy, and (iii) to analyse the implications of applying the P-T formula to agricultural reservoirs and to propose a simplified way to determine the different terms of the formula (i.e., net radiation, heat storage rate and advection coefficient).

STUDY AREA AND MEASUREMENTS

Site and AWR description

The monitored AWR is located at the Experimental Station of the University of Cartagena (south-eastern Spain, 37º35'N, 00º59'W). The Segura River Basin (SRB), within which the facilities lie, is characterized by a Mediterranean semiarid climate, with warm dry summers and mild winters. Climatic data registered at a nearby weather station (Murcia, 38º01'N, 01º10'W) of the Spanish Meteorological Agency (AEMET) provided annual mean values over the period 1985-2007 of 198.1 ± 8.2 W m^{-2} for solar radiation (S), 18.5 ± 0.85 ºC for air temperature (T_a) and 2.16 ± 0.32 m s^{-1} for wind speed (U). Annual rainfall is typically around 350 mm with high seasonal and inter-annual variability; most rain falls during the autumn and winter months (Martinez et al., 2007). The year corresponding to the present study (2007) can be considered representative of the average climate conditions in SRB (annual mean in 2007: S =194.2 W m^{-2}, T_a = 17.8 ºC, U =2.10 m s^{-1}, annual rainfall = 420 mm).

Typical AWRs in South-Eastern Spain are characterized by moderate surface area (from 0.1 to 3 ha), low depth (from 5 to 10m) and waterproof membranes to prevent seepage loss. A detailed description of the characteristics and distribution of irrigation reservoirs in SRB can be found in Martinez *et al*. 2008. The monitored AWR is a small waterproof reservoir, with a maximum depth of 5 m and a surface of 2400 m^2, which can be considered representative of the AWRs commonly used in the region SRB. Evaporation from the AWR water surface was assumed to be the only one uncontrolled water output since seepage was prevented by means of waterproof membranes. The reservoir was filled in January 2007 (initial depth 4.5 m). During the year 2007, there were only small outflows (≈ 0.2 m) for irrigation purposes. These losses and those due to evaporation were partially compensated by rainfall (0.42 m) and a refill (0.50 m) on September 13, performed between 12h and 18 h, when the mean temperature over the water depth (3.5 m) was 23.5 ºC. The latter inflow did not affect significantly the temperature of the water body since the water added for refilling, coming from an underground pipe distribution network connected to the main irrigation canal, was close to 25 ºC.

Climate and evaporation measurements

An automated meteorological station in the vicinity of the AWR provided the climate data for the study. The station is equipped with high quality weather sensors which measure the following meteorological variables 2 m aboveground: air temperature, T_a, and relative humidity, RH (Vaisala HMP45C probe), wind speed, U, (Vector Instruments A100R anemometer), incoming solar radiation, S, (Kipp & Zonen CMP 11 pyranometer) and downward atmospheric radiation, L_a (Kipp & Zonen CGR 3 pyrgeometer). Rainfall was measured by means of a tipping bucket gauge (Young 52203).

The AWR evaporation rate, E (mm day^{-1}) was determined from measurements of the reservoir water level by means of a pressure sensitive transducer (Druck PDCR1830, accuracy = ±0.06% over a 75 mbar range). The sensor was placed in a vessel-connected pipe to facilitate maintenance operations (Figure 1). Data corresponding to days with outflows, rainfall or refilling were discarded from the data analysis, due to the imprecision in measuring or estimating these components. For such days, it was assumed that E was equal to the net radiation of the water surface, expressed in equivalent mm day^{-1}.

Water temperature profiles were obtained by means of six temperature sensors (Campbell T-107) immersed in the water from a floating raft and equidistant 1 m between the water surface and the bottom. An inverted pyranometer (Kipp & Zonen CMP 6) mounted on a steel structure in the raft provided the reflected shortwave radiation, S_r, from which the albedo ($a = S_r/S$) of the water surface was determined. All sensors were scanned at 10 s intervals, hourly averaged and registered by two dataloggers (CR1000 Campbell). The sensors were periodically calibrated. The period of data acquisition covered the whole year 2007.

Figure 1. Dimensions and experimental layout of the monitored AWR

THEORY AND FORMULAE

AWR surface radiative balance

Based on the fundamental physical laws of energy conservation, the radiative balance at the surface of a water body can be expressed as:

$$R_n = (1-a)\ S + L_a - L_w = S_n + L_n \tag{1}$$

where R_n is the net radiation (or available energy) at the water surface, which includes: S_n (= (1 - a) S), the net short-wave radiation, S being the solar radiation and a the albedo of the water, and L_n (= L_a - L_w) the net long-wave radiation, while L_a and L_w are downward and upward long-wave radiation, respectively.

All fluxes, expressed in W m^{-2}, were measured directly, except L_w, which was derived from the data of the temperature sensor located near the surface, T_w, by means of the Stefan-Boltzmann law:

$$L_w = \varepsilon_w \sigma (T_w + 273.2)^4 \qquad (2)$$

where ε_w is the water emissivity, considered to be 0.97 (Ali *et al.*, 2008; Gianniou and Antonopoulos, 2007; Rosenberry *et al.*, 2007), and σ the Stefan-Boltzmann constant (= 5.68 10^{-8} W m^{-2} K^{-4}).

AWR surface energy balance

The energy balance at the surface of a water body can be expressed as the balance of energy gains and losses in a time step (day, month) as follows:

$$R_n + \lambda E + G + H = 0 \qquad (3)$$

where λE is the latent heat flux of evaporation, λ the latent heat of vaporization, where λE is the latent heat flux of evaporation, λ the latent heat of vaporization, G is the heat flux into the underlying water body and H the sensible heat exchanged between the air and the water surface (Brutsaert, 1982). In what follows, both G and H are considered positive when directed towards the surface, and negative when leaving the surface. The available energy is defined as $A = R_n + G$. All daily fluxes are expressed in W m^{-2}, if not mentioned otherwise.

G plays a major role in the changes in stored energy. It can be used as a proxy for the heat storage rate provided that the contribution of the other terms affecting energy storage (heat transfer to substrate and retaining materials, inflows, outflows…) is small and negligible (Gianniou and Antonopoulos, 2007; Rosenberry et al., 2007). Assuming the assumption to hold for the AWR under study, G can be considered equal to the heat storage rate and termed as such in the following.

In our study, daily E was obtained directly from water level measurements and R_n was derived from Equation (1). The sensible heat exchange at the reservoir air–water interface, H, was derived from an analogy between sensible and latent heat transfer. We used the daily mass transfer coefficient h_m (mm day^{-1} kPa^{-1}), defined as:

$$E = h_m (e_w - e_a) \qquad (4)$$

where e_w (kPa) is the saturation vapour pressure at the temperature of the water surface, T_w (ºC), and e_a (kPa) is the vapour pressure of the ambient air. The coefficient h_m was previously calibrated for the studied AWR (Gallego-Elvira *et al.*, 2008). After the required unit conversion, the heat transfer coefficient for sensible heat, h_s (W m^{-2} K^{-1}) was found to be:

$$h_s = 1.88 + 1.48\ U \tag{5}$$

and the daily value of H (W m^{-2}) was calculated as

$$H = h_s(T_a - T_w) \tag{6}$$

The daily Bowen ratio, $\beta = H/\lambda E$, was calculated using the measured values of E and the estimates of H by means of Equation (6).

The heat storage rate, G, was calculated in two different ways: (i) retrieved from Equation (3) as the residual term, once the other terms were known, and (ii) calculated from the daily change in the mean water temperature, T_w (= average of the five temperature sensors) by means of the equation:

$$G = C_w\ z \frac{\Delta T_w}{\Delta t} \tag{7}$$

where C_w (J m^{-3} ºC^{-1}) is the volumetric heat capacity of water at the temperature T_w, z (m) stands for the reservoir depth and ΔT_w is the change in water temperature (ºC) occurring during a time step (Δt = 1day).

Evaporation formulae used in the study

<u>The Penman equation</u>

The Penman equation (Penman, 1948), which is based on the combination of the surface energy balance and an aerodynamic formula, supplies the evaporation rate of a freely evaporating surface by means of the following relationship:

$$\lambda E = \frac{\Delta (R_n + G) + \gamma\, \lambda E_a}{\Delta + \gamma} = w A + (1 - w)\, \lambda E_a = \lambda E_{eq} + \lambda E_{adv} \quad (8)$$

where Δ and γ (kPa K^{-1}) are the slope of the saturated vapour pressure curve at the air temperature and the psychrometric constant, respectively, w stands for the ratio $\Delta/(\Delta + \gamma)$. E_a is the drying power of the air, expressed as the product of a wind function and air vapour pressure deficit. The term $\lambda E_{eq} = wA$ is usually referred to as the *equilibrium* evaporation, or radiative component of the Penman equation. The term $\lambda E_{adv} = (1-w)\ \lambda E_a$ is generally named the *advective*, or aerodynamic component (Brutsaert, 1982). In this study, λE_{adv} was derived from the difference between λE and λE_{eq}.

The Priestley-Taylor formula

The Priestley-Taylor equation (1972) is formulated as a truncated version of the Penman equation:

$$\lambda E = \alpha \frac{\Delta}{\Delta + \gamma} (R_n + G) = \alpha\ w A = \alpha\ \lambda E_{eq} \quad (9)$$

with

$$\alpha = 1 + E_{adv}/E_{eq} \quad (10)$$

The coefficient α, or advection coefficient, reflects the importance of the advective component with respect to the radiative one. α can be considered as a lumped parameter, which includes the aerodynamic term of the Penman equation and, consequently, integrates the effects of several climatic and surface-related factors, such as the vapour pressure deficit, the wind speed, surface roughness and water body characteristics.

RESULTS AND DISCUSSION

The yearly evolution and the annual characteristics (annual mean, maximum, and minimum values and range of the monthly values of the AWR radiative balance terms (Equation (1)) are given in Figure 2 and Table I. They indicate that downward long wave radiation, L_a, was the main energy input (394.4 W m^{-2}), doubling the influx from solar radiation (194.2 W m^{-2}). However, the amplitude in the annual variation of S (= 218 W m^{-2}) was more than twice that of L_a (= 94 W m^{-2}) (Figure 2). As regards heat losses, the upward long wave radiation, L_w, was the main energy output (=412.6 W m^{-2}), accounting for 97% of the total loss (424.6 W m^{-2}), while the reflected solar radiation only accounted for 3% (12 W m^{-2}). The latter exhibited a smother seasonal variation than S, since periods with higher solar radiation months coincided with those of lower albedo values. A clear cyclic pattern of albedo was observed (Figure 3), with a minimum of 0.04 around the summer solstice (June) and a maximum of 0.11 at the winter solstice (December). This behaviour can be logically ascribed to the variation of the solar elevation angle. The albedo values were fitted (minimum MAE) to the following simple sinusoidal function of the month of the year, M (= 1, ...12), with a fairly good result (Figure 2, MAE = 0.0024, RMSE = 0.0033):

$$\mathrm{a} = \mathrm{a_o} + \mathrm{b}\sin\left(2\pi\left(M + c\right)/12\right) \tag{11}$$

being a_o, b and c constants with the following values: a_o = 0.0718 (unitless). b = 0.0325 (unitless) and c = 3.08 (month unit).

Table I. Annual mean, minimum, maximum and range of the monthly values of the components of the AWR radiative balance (Units=W m^{-2})

Figure 2. Annual evolution of the components of the radiative balance (monthly values). Positive and negative values correspond to energy inputs and outputs to the AWR, respectively. Vertical bars are standard deviations of the daily values.

Figure 3. Annual cycle of the surface albedo (monthly values). Points represent the ratio of the monthly means of reflected and incoming solar radiation, the dotted curve is the sinusoidal function described by Equation (11). The dashed line is the constant a_o = 0.0718, representative of the mean annual albedo.

The respective peaks of L_a and L_w occurred in August, with a delay of about 1 to 2 months with respect to the maximum of S (Figure 2). The net long wave radiation L_n presented a small annual variation range (- 82.2 W m^{-2} < L_n < -26.4 W m^{-2}) (Table I). Conversely, the net short-wave radiation S_n presented a rather wide range of variation (85.6 W m^{-2} < S_n < 300.0 W m^{-2}), with an annual pattern very close to S (94.7 W m^{-2} < S

< 313.1 W m^{-2}) because of the small and quite constant values of the reflected solar radiation, *aS* (Table I). The net radiation R_n ranged from 20.0 W m^{-2} (Dec) to 217.8 W m^{-2} (July), with an annual amplitude of 197.8 W m^{-2}, close to the annual amplitude of S (218.4 Wm^{-2}) (Table I). Note that the ratio $r = R_n/S$ was 0.61 on an annual basis, with a sharp difference between June and July ($r \approx 0.70$) and December ($r \approx 0.20$). There was a close relationship between R_n and S ($R_n = 0.86\ S - 48.13$, $R^2 = 0.97$), with a hysteretic trend for the period from October to March. The latter can be explained by the asymmetrical pattern of the long wave radiative components, L_a and L_w (Figure 2).

Energy balance

The annual mean, minimum, maximum and amplitude of the monthly values of the components of the AWR energy balance (Equation (3)) are given in Table II. The annual pattern of the monthly mean is presented in Figure 4 for each component.

<u>Evaporation rate</u>

For the year of observation, the annual latent heat flux of the studied AWR was 102.7 W m^{-2}, equivalent to an evaporated water depth of 1310 mm $year^{-1}$. The evaporation rate peaked in July, with a value of 183.7 W m^{-2}, while the lowest monthly value (= 35.3 Wm^{-2}) was observed in December (Figure 4). Note that evaporation loss for March was higher than that registered for April, due to the particularly windy weather prevailing in March. In fact, the two highest evaporation values were observed on 8 March (13.3 mm day^{-1}) and on 20 March (10.7 mm day^{-1}), both substantially higher than the maximum value (9.7 mm day^{-1}) of the summer period, observed on 24 August.

Table II. Annual mean, minimum, maximum and amplitude of the monthly values of the components of the AWR energy balance ($\lambda E, H, G, R_n, A$), evaporative fraction (EF), Bowen ratio (β), equilibrium and advective components (λE_{eq} and λE_{adv}) and advection coefficient (α). Values of G correspond to the residual of the energy balance (G_{EB})

Figure 4. Annual evolution of the components of the energy balance (monthly average). Values of G correspond to those retrieved from the surface energy balance (residual value). Vertical bars are standard deviations of the daily values.

Sensible heat flux and Bowen ratio

The sensible heat flux was relatively small compared with the other components (annual mean = 10.6 W m^{-2}, Table II), with a maximum in July (17.1 W m^{-2}) and a minimum in February (-0.1 W m^{-2}). Except for the last value, the Bowen ratio was quite stable throughout the year, varying in the range 0.10 – 0.20 (Figure 5). β was close to 0.10 during the warm season, with only very small variations, while greater variability was observed in the winter months. This was due to the occurrence of negative values for β, corresponding to very cloudy conditions and low available energy. The order of magnitude of β agreed well with previous published estimations for β in small water storages in semiarid locations and flooded fields. The annual mean of β was found to be 0.07 for a small pond in Badakhera watershed in India (4700 m^2, depth 2.75m) (Ali *et al.*, 2008). For larger and deeper water bodies under different climatic conditions, higher annual values of β have been documented: 0.19 for Lake Ikeda in Japan (10.62 km^2, mean depth 125 m) (Momii and Ito, 2008), 0.21 for Lake Titicaca in South America (8560 km^2, mean depth 105 m) (Delclaux *et al.*, 2007) and 0.23 for Sparkling Lake in USA (0.64 km^2, mean depth 10.9 m) (Lenters *et al.*, 2005). These higher values were generally associated with a wider range of monthly β as, for instance, in lake Ikeda ($-0.1<\beta< 0.4$) and Sparkling Lake ($0.09 <\beta < 0.85$).

Figure 5. Annual evolution of the Bowen ratio (monthly values). Vertical bars are standard deviation of the daily values

Our results highlight the fact that the reservoir heated the surrounding atmosphere during the whole year, except in February. It appears that the water reservoir acted in the same way as a solar collector with a notable capacity of seasonal storage, absorbing energy during the spring and summer season and releasing it during the fall season to reach an equilibrium state with the atmosphere ($T_w \approx T_a$) in February. This month therefore corresponds to the time of year when the energy buffer due to the heat stored during the previous spring and summer became completely exhausted and to the start for a new annual cycle of heat storage. Note also that February was the only month for which the evaporative fraction EF (= $\lambda E/A$) was equal to 1, i.e. all the available energy was used for the evaporation process.

Heat storage rate, G

The evolution of G was characterized by an annual cycle (Figure 4), with a 6-month period of storage (from February to July) followed by another 6-month period of release (from August to January). The peak of G, calculated as the residual term of the energy balance equation, G_{EB}, was observed in April (≈ 50 W m^{-2}) while the maximum release rate (≈ 40 W m^{-2}) occurred during the months of October and November. The annual cycle of G can be described by a sinusoidal function (Figure 6). Note the relatively large deviation from the sinusoidal trend occurring in March, when strong winds notably increased the evaporation rate and led to a low magnitude of stored energy compared with February and April.

Figure 6. Annual cycle of the heat storage rate, G_{EB}, derived from the energy balance (monthly values). Negative values correspond to heat storage rate. The dotted line is the best fit to the sinusoidal function: $G_{EB}= a_w + b_w (sin(2\pi(M + c_w)/12$, with a_w = -6.95 W m^{-2} (dashed line), b_w = 42.98 W m^{-2} and c_w = 4.62 (MAE = 7.76 W m^{-2}, RMSE = 12.18 W m^{-2})

The comparison between G_{EB} and the estimates of G deduced from the vertical temperature profile, G_{WT} (Equation (7)), indicated fairly good agreement between the two methods (G_{WT} = 0.94 G_{EB} + 6.39, R^2 = 0.97).

Partitioning of available energy

As regards the annual energy balance values (Table II), the available energy (A = 113.3 W m^{-2}) was close to and slightly lower than the net radiation (R_n = 118.9 W m^{-2}), the difference (-5.6 W m^{-2}) being partly due to the small value of residual heat storage rate observed in December (T_w = 12.5 ºC) with respect to that observed in January (T_w = 12.2 ºC). The annual evaporative fraction was equal to 0.91 (Table II), and the ratio H/A to 0.09.

At the monthly scale, there was a very close correlation between λE and A (Figure 7a, λE = 0.909 A, R^2 = 0.997, for the regression forced to the origin) and also a significant linear relationship between H and A (Figure 7b, $H = 0.091\ A$. $R^2 = 0.72$). The heat accumulated by the water body during the spring and the beginning of summer was released in the autumn, increasing the energy available for evaporation. As a consequence, the net radiation and the evaporation rate are somewhat decoupled and show a clear hysteretic trend (Figure 8).

Figure 7. Relationship between available energy, A, and (a) λE, (b) H (monthly values). The line corresponds to the regression forced to the origin (a) $\lambda E = 0.909\ A$, $R^2 = 0.997$ (b) $H = 0.091\ A$. $R^2 = 0.72$

Figure 8. Hysteresis between evaporation, λE, and net radiation, R_n(monthly values). The line corresponds to the regression: $\lambda E = 0.72\ R_n + 19.7$, $R^2 = 0.83$

The hysteresis loop between λE and R_n could lead to systematic errors if the heat storage term in radiation based formulae that aim to estimate evaporation from climatic data is not considered.

<u>Partitioning between equilibrium and advective evaporation</u>

There was a clear predominance of the equilibrium term, λE_{eq} , over the advective term, λE_{adv} during the warm period of the year when λE_{eq} represented approximately 80% of λE (Figure 9). During the winter months, the advective term reached about one third of the total evaporation, with a maximum of 40% in February. This maximum coincided with a Bowen ratio near 0.

Figure 9. Annual evolution of evaporation flux, equilibrium and advective evaporation terms of the Penman formula and available energy (monthly values).

Implications for evaporation estimates with the P-T formula

<u>Advection coefficient, α</u>

On a yearly scale, the equilibrium, λE_e, and advective, λE_{adv}, evaporation terms of the Penman formula (Equation (8)) represented 76% and 24%, respectively, of the total evaporation (Table II), leading to an annual value for α (Equation (10)) of 1.32. This is within the range (1.15 to 1.45) reported in the literature (Debruin and Keijman, 1979); Morton 1983; Pereira and Villa Nova, 1992; McAneney and Itier, 1996: Hobbins *et al.*, 2001), and close to the standard value of 1.26. Values proposed by Doorenboos and Pruitt (1977) for irrigated crops ranged between 1.33 and 1.46, while higher values of up to 1.74 (Jensen *et al.*, 1990) were reported for arid and warm countries.

On a monthly scale, the range was quite large ($1.23 < \alpha < 1.65$, Table II), with α showing a clear seasonal pattern (Figure 10). The lowest values were obtained for the summer months (June-July-August), while the maximum value was observed in February. The daily values for α varied very little from May to October, but showed high variability from December to February (Figure 10).

Neglecting the storage component (i.e. assuming $A \approx R_n$), a R_n-based advection coefficient, α*, was calculated. The use of such a coefficient on an annual scale provided a value for α* of 1.25, which is close to the value of 1.32 obtained for α. This result was to be expected, as the annual value of R_n was only 5% higher than the annual value of *A* (Table II). However, there were significant differences between monthly α and α* (Figure 10), especially during the autumn, when the energy release rate was high (Oct-Nov-Dec). The range of variation of α*($0.90 < \alpha^* < 3.26$) was rather unrealistic, demonstrating the importance of accounting for *G* in estimating the annual evolution of α.

Figure 10. Annual evolution of the advection coefficient, α, and of its equivalent based on net radiation, α* (see text for explanation, monthly values). The dotted line is the constant value α = 1.26. Vertical bars are standard deviation of the daily values of α

One way of obtaining a plausible estimation of α would be to use the direct relationship linking α to the Bowen ratio:

$$\alpha = \frac{\Delta + \gamma}{\Delta(1+\beta)} = \frac{1}{w(1+\beta)} \qquad (12)$$

As β was found to be relatively constant throughout the year ($\beta = 0.103 \pm 0.051$, Figure 5), we assumed $\beta = 0.10$ in Equation (12), which then becomes:

$$\alpha = 0.91 w^{-1} \qquad (13)$$

Figure 11 shows how the hyperbola corresponding to Equation (13) fits the observed monthly values of α. Using Equation (13) to predict the observed values of α would lead to a mean absolute error (MAE) of 0.045 and a root mean square error (RMSE) of 0.066, which could be considered rather satisfactory.

Figure 11. Experimental monthly values of α and Equation 13 (dotted curve) vs. $w = \Delta/(\Delta+\gamma)$. RMSE = 0.066, MAE = 0.045

Alternative to estimate *G*

The proper way of predicting *G* is by means of Equation (7), whose evolution can be described by the sinusoidal function presented in Figure 7. Equation (7) requires measurements of water temperature, which are often unavailable. A candidate to substitute water temperature is air temperature, T_a. In fact, in several studies, a regression equation is used to predict T_w from T_a data (Ali *et al*., 2008; Mohseni and Stefan, 1999). In our study T_a showed a close correlation with T_w (R^2 = 0.99, data not shown). A linear regression between G_{WT} and $\Delta T_{a,j}$ (the change in monthly temperature between two consecutive months) is proposed to derive *G* when T_w is not available (Figure 12).

$$G_{WT} = -7.98\ \Delta T_{a,j} + 0.16 \qquad (14)$$

with R^2 = 0.83 and MAE = 7.42 W m^{-2}. Correlations with other variables, such as net and solar radiation, or air vapour pressure deficit, were analysed and found to be much less satisfactory (results not shown).

Figure 12. Relationship between G_{WT} and the change in monthly air temperature between two consecutive months, $\Delta T_{a,j}$. Negative values of G_{WT} correspond to storage. The line is the regression $G_{WT} = -8.55\ \Delta T_{a,j} - 5.63$, $R^2 = 0.84$ (Equation 14)

Alternative to estimate R_n

To apply the P-T equation, a knowledge of R_n is necessary. A common option is to use the procedure recommended by the FAO (Allen *et al*., 1998). The monthly values of albedo from Equation (11) can be applied, although the use of an average value of 0.07 could be sufficient, since the reflected solar component represents only a small fraction (3%) of the total radiative losses. More critical is the use of air temperature as a proxy for water temperature in calculating long-wave radiation emitted by the surface. Differences of up to 3ºC were observed between T_w and T_a, which would be equivalent to an error of 15 W m^{-2} in the estimate of the net long wave radiation when assuming $T_w = T_a$. Therefore, water temperature measurements are recommended if the FAO method is to be used. An alternative option would be to use a relationship between R_n and S, such as the linear regression found in this study which could be applied for small AWRs under semi-arid climate conditions.

CONCLUSIONS

Although inter-annual variability can affect to some extent the evolution of the energy balance and hence evaporation rate, the results of this study provide a good understanding of the average behaviour of small on-farm storage reservoirs under Mediterranean semiarid conditions. Overall, our results indicate that the annual evaporation loss of small irrigation reservoirs in semi-arid climates presents an order of magnitude that is close to the regional potential evaporation as defined by Priestley and Taylor (1972) for temperate and humid climates. The annual advection coefficient, α, was found to be within the range of values currently assumed for temperate regions ($1.20 < \alpha < 1.35$), and similar to that reported for small ponds under semiarid weather conditions. It seems therefore that, despite its limited area (2500 m^2), the AWR under study provides a proxy of the areal potential evaporation. The order of magnitude of the Bowen ratio ($\beta \approx 0.10$) and its range variation ($0 < \beta < 0.20$) agreed well with previous published estimations for small water storages and flooded fields in semiarid locations, confirming that evaporation is by far the main process responsible for cooling of small open water bodies.

On a monthly scale, our experimental study highlights the importance of considering the annual cycle of both heat storage and advection coefficient. As far as these two issues are concerned, the results of our study can be summarised as follows:

1) For the AWR under study, heat storage led to an annual pattern of available energy quite distinct from that observed for R_n. In spring and early summer, the fraction of net radiation stored in the water mass decreased the amount of energy available to the evaporation process, while during the autumn, a significant fraction of the net radiation energy that was stored in the water body during spring and early summer became available to the evaporation process. Therefore, the approximation $A = R_n$ could lead to significant errors, as stressed by Finch (2002). To properly predict the monthly evaporation rate, heat storage should be accounted for, either directly from measurements or indirectly by means of empirical relationships. When water temperature measurements are not available, we suggest estimating G by means of a relationship linking G to the air temperature difference between two consecutive months (Equation (14)).

2) The advection coefficient of the P-T formula presented a marked annual cycle due to the hysteretic trend observed between R_n and λE. The enhanced role of the advection process observed in autumn and winter could be corrected by including a seasonal variation of the advection coefficient, α. Our proposal, for this type of AWR with a rather constant Bowen ratio (≈ 0.1), is to calculate α from a functional relationship linking α to β, assuming $\beta = 0.1$. This appears to be a straightforward way to include the effects of seasonal changes of α in the AWR evaporation loss predicted by the P-T formula.

ACKNOWLEDGEMENTS

The authors acknowledge the Fundación Séneca (Murcia, Spain) for the financial support of this study through the grant 02978/PI/05.

REFERENCES

Ali S, Ghosh NC, Singh R. 2008. Evaluating best evaporation estimate model for water surface evaporation in semi-arid region, India. *Hydrological Processes* **22**: 1093-1106. DOI: 10.1002/hyp.6664.

Allen RG, Pereira LS, Raes D, Smith M. 1998. *Crop Evapotranspiration: Guidelines for Computing Crop Water Requirement, FAO Irrigation and Drainage Paper* No. 56. Food and Agricultural Organization of United Nations: Rome.

Brutsaert W. 1982. *Evaporation into Atmosphere: Theory, History, and Applications*. D. Reidel Publishing Company: Boston, MA.

Craig I, Green A, Scobie M, Schmidt E. 2005. *Controlling Evaporation Loss from Water Storages.* NCEA Publication No. 1000580/1: Queensland; 207.

Daigo K, Phaovattana V. 1999. Evaporation and percolation control in small farm ponds in Thailand. *JARQ-Japan Agricultural Research Quarterly* **33**: 47-56.

Debruin HA, Keijman JQ. 1979. Priestley-Taylor Evaporation Model Applied to A Large, Shallow Lake in the Netherlands. *Journal of Applied Meteorology* **18**: 898-903.

Delclaux F, Coudrain A, Condom T. 2007. Evaporation estimation on Lake Titicaca: a synthesis review and modelling. *Hydrological Processes* **21**: 1664-1677. DOI: 10.1002/hyp.6360.

Doorenbos J, Pruitt WO. 1977. *Guidelines for predicting crop water requirements. FAO Irrigation and Drainage* Paper No. 24: Rome; 179.

Downing JA, Prairie YT, Cole JJ, Duarte C.M, Tranvik LJ, Striegl RG, McDowell WH, Kortelainen P, Caraco NF, Melack JM, Middelburg JJ. 2006. The global abundance and size distribution of lakes, ponds, and impoundments. *Limnology and Oceanography* **51**: 2388-2397.

Finch JW. 2001. A comparison between measured and modelled open water evaporation from a reservoir in south-east England. *Hydrological Processes* **15** 14: 2771-2778.

Finch JW, Gash JHC. 2002. Application of a simple finite difference model for estimating evaporation from open water. *Journal of Hydrology* **255**: 253-259.

Gallego-Elvira B, Baille A, Martínez-Álvarez V, Martín-Górriz B. 2008. Pan coefficient and wind function of agricultural water reservoirs under a semi-arid climate. *Proceedings of International Conference on Agricultural Engineering and Industry Exhibition,* June 2008, Crete, Greece.

Gianniou SK, Antonopoulos VZ. 2007. Evaporation and energy budget in lake Vegoritis, Greece. *Journal of Hydrology* **345** : 212-223. DOI: 10.1016/j.jhydrol.2007.08.007.

Hobbins MT, Ramirez JA, Brown TC, Claessens LHJM. 2001. The complementary relationship in estimation of regional evapotranspiration: The Complementary Relationship Areal Evapotranspiration and Advection-Aridity models. *Water Resources Research* **37**: 1367-1387.

Hudson NW. 1987. *Soil and Water Conservation in Semiarid Regions*. FAO Land and Water Conservation Service: Rome; 256.

Jensen ME, Burman RD, Allen RG. 1990. *Evapotranspiration and Irrigation Water Requirements.* ASCE Manuals and Reports of Engineering Practice No. 70. ASCE: New York.

Lenters JD, Kratz TK, Bowser CJ. 2005. Effects of climate variability on lake evaporation: Results from a long-term energy budget study of Sparkling Lake, northern Wisconsin (USA). *Journal of Hydrology* **308**: 168-195. DOI: 10.1016/j.jhydrol.2004.10.028.

McAneney KJ, Itier B. 1996. Operational limits to the Priestley-Taylor formula. *Irrigation Science* **17**:37-43.

Martínez-Alvarez V, Baille A, Molina-Martínez JM, González-Real MM. 2006. Efficiency of shading materials in reducing evaporation from free water surfaces. *Agricultural Water Management* **84**: 229-239. DOI: 10.1016/j.agwat.2006.02.006.

Martinez-Alvarez V, Gonzalez-Real MM, Baille A, Molina-Martínez JM. 2007. A novel approach for estimating the pan coefficient of irrigation water reservoirs application to South Eastern Spain. *Agricultural Water Management* **92**: 29-40. DOI: 10.1016/j.agwat.2007.04.011.

Martínez-Alvarez V, González-Real MM, Baille A, Maestre-Valero JF, Gallego-Elvira B. 2008. Regional Assessment of Evaporation from Agricultural Irrigation Reservoirs in a Semiarid Climate. *Agricultural Water Management* **95**: 1056-1066. DOI: 10.1016/j.agwat.2008.04.003

Mohseni O, Stefan HG. 1999. Stream temperature air temperature relationship: a physical interpretation. *Journal of Hydrology* **218**: 128-141.

Momii K, Ito Y. 2008. Heat budget estimates for Lake Ikeda, Japan. *Journal of Hydrology* **361**: 362-370. DOI: 10.1016/j.jhydrol.2008.08.004.

Morton FI. 1983. Operational estimates of areal evapotranspiration and their significance to the science and practice of hydrology. *Journal of Hydrology* **66**: 1–76.

Penman HL. 1948. Natural Evaporation from Open Water, Bare Soil and Grass. *Proceedings of the Royal Society of London Series A-Mathematical and Physical Sciences* **193**: 120-&.

Pereira AR, Villa Nova NA. 1992, Analysis of the Priestley-Taylor parameter: *Agricultural and Forest Meteorology* **61**: 1-9.

Priestley CHB, Taylor RJ. 1972. On the assessment of surface heat flux and evaporation using large scale parameters. *Monthly Weather Review* **100**: 81–92.

Rosenberry DO, Winter TC, Buso DC, Likens GE. 2007. Comparison of 15 evaporation methods applied to a small mountain lake in the northeastern USA. *Journal of Hydrology* **340**: 149-166. DOI: 10.1016/j.jhydrol.2007.03.018.

Sacks LA, Lee TM, Radell MJ. 1994. Comparison of Energy-Budget Evaporation Losses from 2 Morphometrically Different Florida Seepage Lakes. *Journal of Hydrology* **156**: 311-334.

Table I. Annual mean, minimum, maximum and range of the monthly values of the components of the AWR radiative balance (Units=W m^{-2})

	S	aS	S_n	L_a	L_w	L_n	R_n	R_n/S	a
Mean	194.2	12.3	181.9	349.4	412.7	-63.2	118.9	0.61	0.072
Max	313.1	9.1	300.0	396.5	368.9	-26.4	217.8	0.70	0.115
Min	94.7	14.5	85.6	302.1	460.8	-82.2	20.0	0.20	0.042
Range	218.4	5.4	214.4	94.4	91.9	55.8	197.8	0.50	0.073

Table II. Annual mean, minimum, maximum and amplitude of the monthly values of the components of the AWR energy balance ($\lambda E, H, G, R_n, A$), evaporative fraction (EF), Bowen ratio (β), equilibrium and advective components (λE_{eq} and λE_{adv}) and advection coefficient (α). Values of G correspond to the residual of the energy balance (G_{EB}).

	λE	H	G	R_n	A	EF	β	λE_{eq}	λE_{adv}	α
Mean	-102.7	-10.6	-5.6	118.9	113.3	0.91	0.103	78.0	24.7	1.32
Max	-183.7	-17.1	41.1	217.8	200.1	1.00	0.203	149.2	35.8	1.65
Min	-35.3	0.1	-49.0	20.0	37.6	0.83	-0.003	21.9	12.3	1.23
Range	148.4	17.2	90.1	197.8	162.5	0.17	0.206	127.3	23.5	0.42

Figure 1

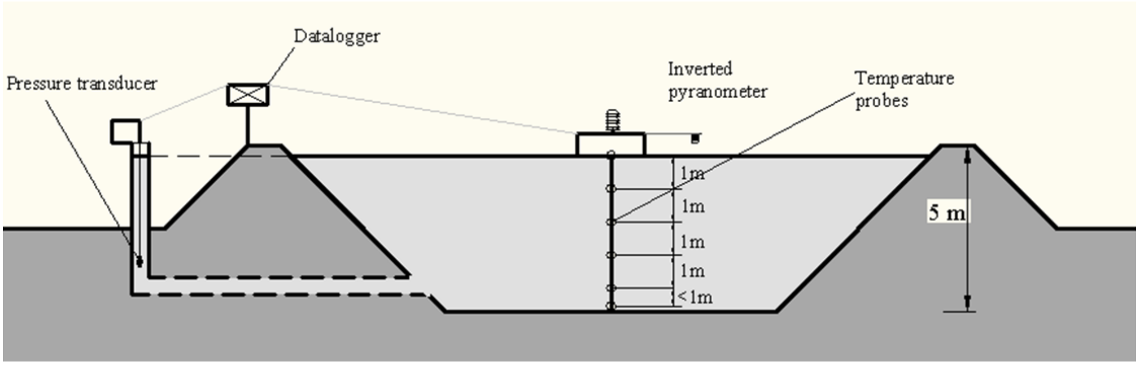

Figure 2

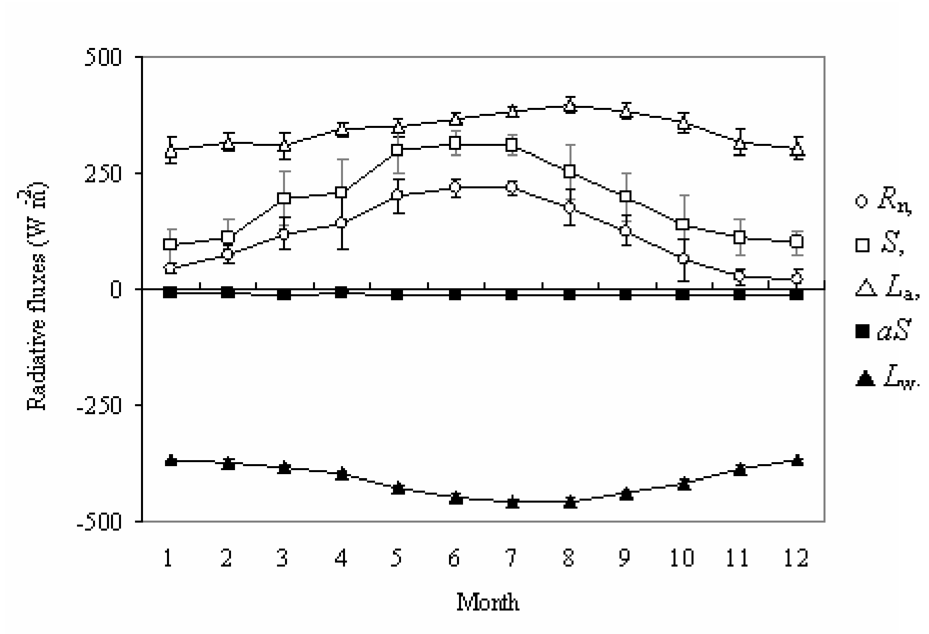

Figure 3

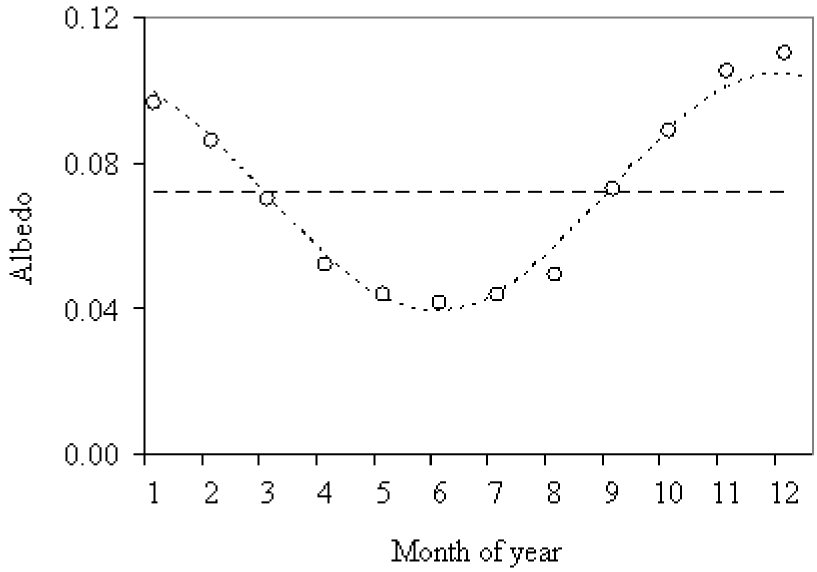

Figure 4

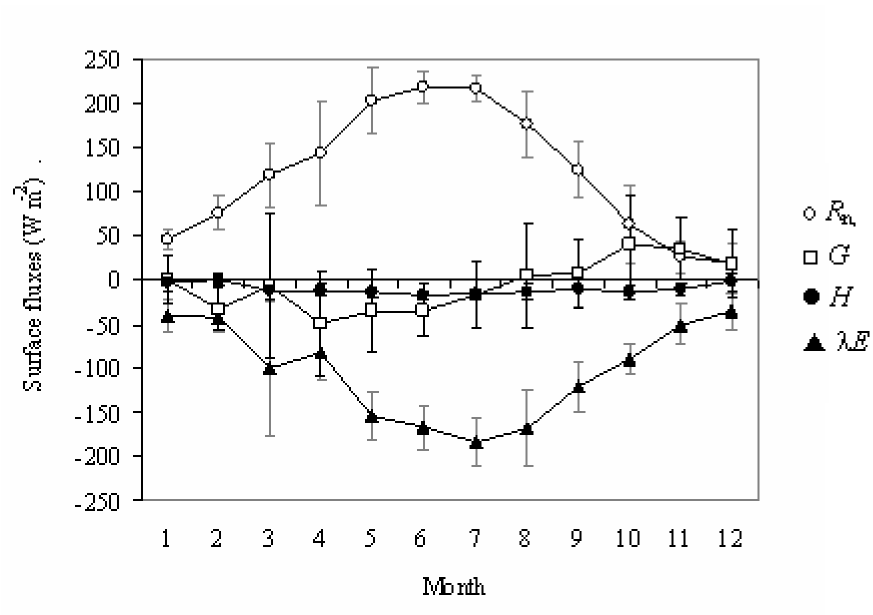

Figure 5

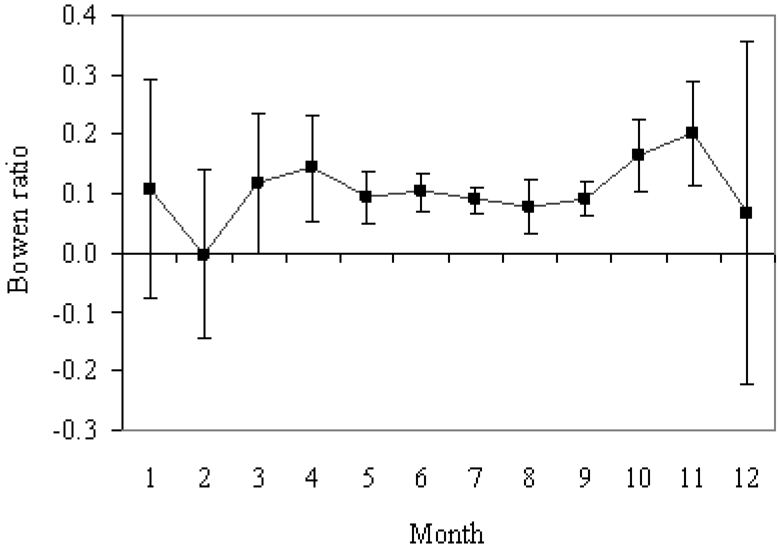

Figure 6

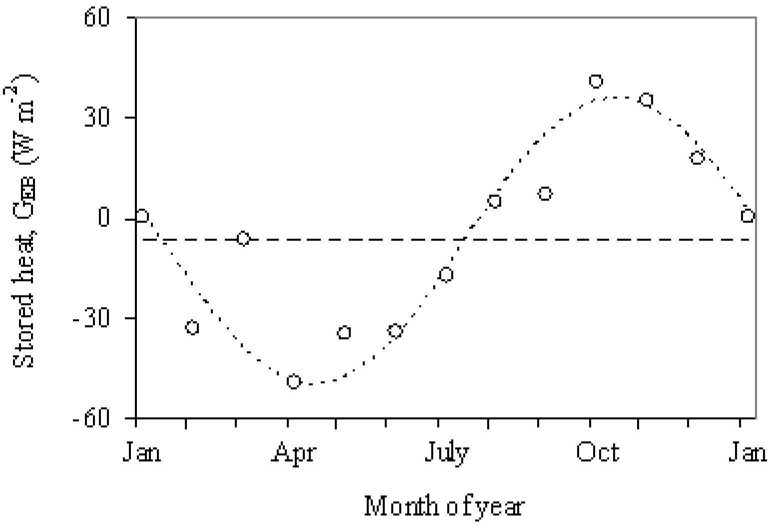

Figure 7

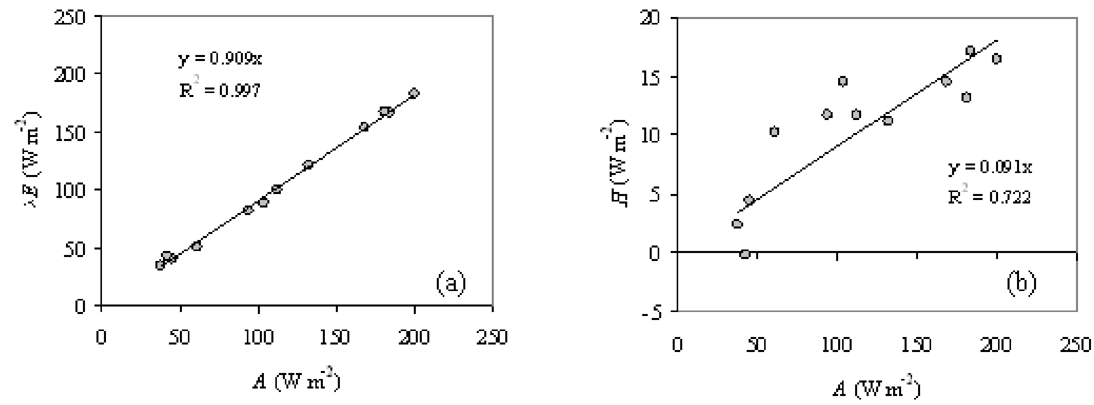

Figure 8

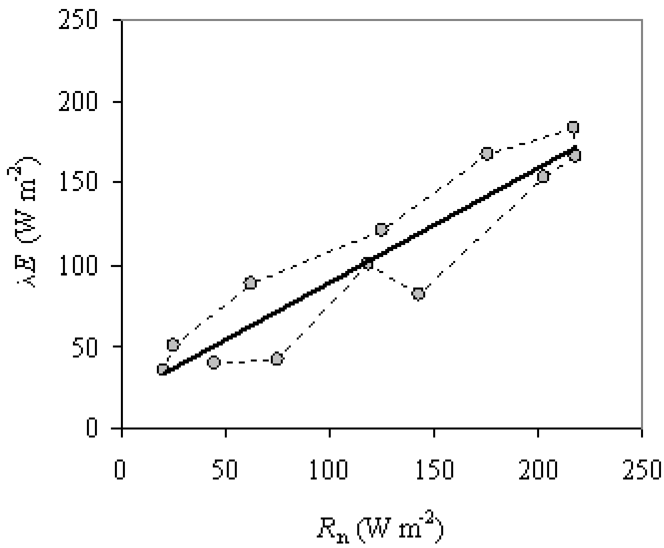

Figure 9

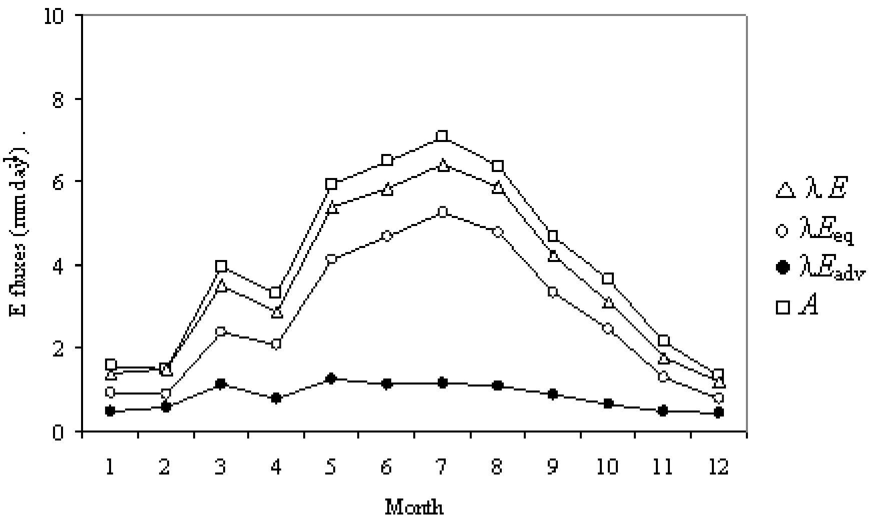

Figure 10

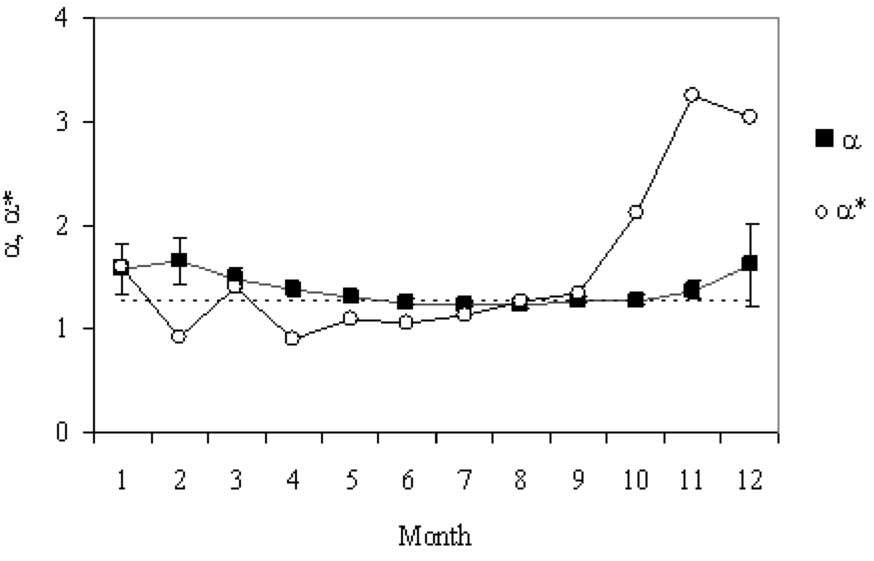

Figure 11

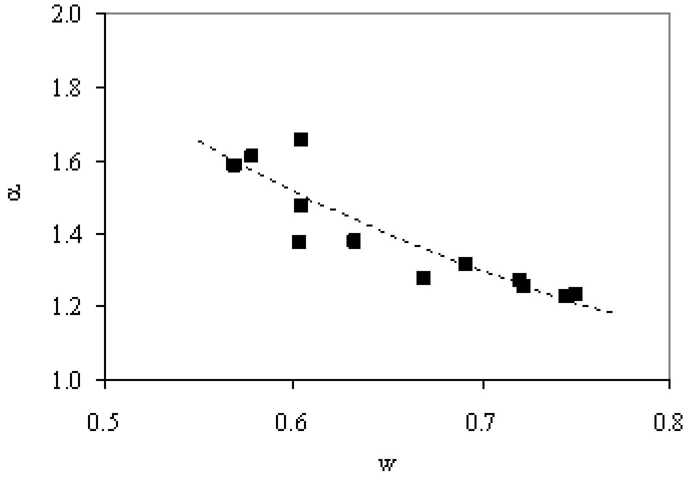

Figure 12